Journal of Membrane Science, 77 (1993) 165–179
Elsevier Science Publishers B.V., Amsterdam

SDI 0376-7388(93)

"Ultramicroporous" silica-based supported inorganic membranes

C.J. Brinker[a,b], T.L. Ward[b], R. Sehgal[b], N.K. Raman[b], S.L. Hietala[b], D.M. Smith[b], D.-W. Hua[b] and T.J. Headley[a]

[a]*Ceramic Synthesis and Inorganic Chemistry Department 1846, Sandia National Laboratories, Albuquerque, NM 87185 (USA)*

[b]*The UNM/NSF Center for Micro-Engineered Ceramics, University of New Mexico, Albuquerque, NM 87131 (USA)*

(Received June 1, 1992; accepted in revised form September 25, 1992)

Abstract

Ultramicroporous (Pore radius <10 Å) separation layers with thicknesses in the range of 200–1200 Å were deposited from polymeric silicate sols onto commercial alumina supports using a dip-coating/casting procedure. The silicate sols were prepared using a two-step acid-catalyzed hydrolysis of tetraethoxysilane under pH conditions where the condensation rate is low, producing polymers of low fractal dimension which readily interpenetrate during film deposition to provide amorphous layers with extremely small pore sizes. At low aging times ($t/t_{gel}=0.05$), the acid catalyst concentration had a dramatic effect on the deposited membrane permeability. Using 1*N* HCl a discrete, featureless membrane layer was deposited on top of the mesoporous support (as revealed by TEM), while lower acid concentration (0.44 *N*) resulted in polymer penetration and filling of the support pores rather than the deposition of a discrete external layer. This was attributed to the effect of acid concentration on the polymer condensation rate during the final stages of membrane deposition and drying. Deposited membrane layer thickness was found to depend on sol aging time, solvent dilution, and dipping/casting time. Helium permeabilities for deposited layers were ~ 1000–2000 barrer. Measured reductions (65–90%) in the helium and nitrogen permeation rates upon membrane deposition indicated pore radii less than 10 Å for the deposited membrane layers.

Keywords: microporous membranes; silica-based membranes; sol-gel process; permeability

1. Introduction

Owing to their presumed greater thermal, mechanical, and chemical stability, inorganic membranes have been proposed as replacements for conventional organic polymer membranes in a variety of applications such as high temperature gas separation and catalytic membrane reactors [1]. At high temperatures facilitated transport mechanisms such as selective adsorption or capillary condensation are generally not operative, so membrane selectivity is related mainly to pore size and pore size distribution. Most high temperature applications require so-called "ultramicroporous" membranes, i.e. those with sufficiently small pores

Correspondence to: C.J. Brinker, Ceramic Synthesis and Inorganic Chemistry Department 1846, Sandia National Laboratories, Albuquerque, NM 87185, USA. Fax: +1 505-277-0813.

(<0.1 nm) that molecules are admitted or excluded on the basis of size by molecular sieving.

1.1. Particulate versus polymeric sols

The conventional route to preparing asymmetric, supported, inorganic membranes is the sequential deposition of particulate sols with narrow particle size distributions [2–4]. If aggregation is avoided, the pore size of the membrane is controlled by the particle size of the sol – smaller particles yield smaller pores. The advantage of this approach is that the porosity of the membrane (which dictates its flux) is independent of the particle size. For example, random dense packing of monosized particles always results in about 33% porosity. There are however several disadvantages of the particulate approach in achieving ultramicroporous membranes:

(1) Most commonly, in order to avoid aggregation, an electrostatic double layer is erected around each particle, If, according to DLVO theory, we use the Debye–Hückel screening length $1/\kappa$ to judge the thickness of the double layer [5]:

$$1/\kappa = 1/(F^2 \sum_i c_i z_i^2 / \epsilon \epsilon_o RT)^{1/2} \quad (1)$$

where F is Faraday's constant, ϵ_o is the permittivity of vacuum, ϵ is the dielectric constant of the solvent, T is the temperature, and c_i and z_i are the concentration and valence of counterions of type i, we see that it does not depend directly on particle size. This is problematic when using very small particles, since, as the particle size is diminished, the tightly bound solvent layer comprises an ever increasing volume fraction of the deposited film. The removal of this liquid during drying at elevated temperatures creates tensile stresses σ within the plane of the membrane that results in cracking:

$$\sigma = [E/(1-\nu)][(f_s - f_r)/3], \quad (2)$$

where E is Young's modulus (Pa), ν is Poisson's ratio, f_s is the volume fraction solvent at the solidification point, and f_r is the residual solvent (if any) in the fully dried film. From eqn. (2) we see that σ is directly proportional to f_s. The result is that cracking is more likely to occur in particulate membranes as the particle size is reduced [6].

(2) Many of the particles currently used (TiO_2, Al_2O_3, ZrO_2, AlOOH, etc.) undergo phase transformations and/or grain growth at relatively low temperatures, causing the microstructure to coarsen significantly [7]. This is problematic when attempting to prepare stable, ultramicroporous membranes.

(3) As the particle radius r is reduced the particle solubility S increases according to the Ostwald–Freundlich equation:

$$S = S_0 \exp(2\gamma_{SL} V_m / RTr) \quad (3)$$

where S_0 is the solubility of a flat plate, γ_{SL} is the solid–liquid interfacial energy, and V_m is the molar volume of the solid phase. As the particle size is reduced below 5 nm, S increases dramatically. Thus in many liquid environments ultramicroporous particulate films are inherently unstable.

A second approach to the preparation of supported, ultramicroporous, inorganic membranes utilizes polymeric sols, i.e. those composed of less highly branched clusters that do not contain a fully condensed ceramic core. Often such species are formed in solution via sol–gel processing [8] by kinetically limited growth processes [9], and their structures are characterized by a mass fractal dimension D which relates the cluster mass M to its radius r_c according to [10]:

$$M \propto r_c^D \quad (4)$$

where in three dimensions, $0 < D < 3$.

The principle advantages of polymeric sols are that they avoid the three disadvantages of particulate sols listed above: (1) Aggregation may be exploited to tailor porosity of deposited

membranes, (2) most polymeric sols form amorphous phases that do not suffer phase transitions or grain growth when heated to moderate temperatures, and (3) the interpenetrating polymeric networks create roughly cylindrical pores with negative radii of curvature ($r<0$ in eqn. 3), causing the dissolution rate to decrease dramatically with decreasing pore size. A possible disadvantage is that small pore sizes are created by a collapse of the network, resulting in low volume fraction porosities and correspondingly low fluxes. It is necessary therefore to prepare inorganic polymer membranes in ultrathin film form (<100 nm).

1.2. Control of pore size using polymeric sols

When preparing a membrane by slip-casting or dip-coating from a polymeric sol, the pore size and pore volume depend on the structure of the inorganic polymers (e.g. size and mass fractal dimension), the reactivity of these species (e.g. the condensation or aggregation rates), the time scale of the deposition process (related to the casting time, substrate withdrawal rate, and film thickness), and the magnitude of the shear forces and capillary forces that accompany membrane deposition (related to the surface tension of the solvent and possible surface tension gradients in mixed solvents) [11]. See Fig. 1. In the initial stages of sol deposition, slip-casting is the dominant mechanism as fluid is drawn into the porous support due to capillary forces. In the final stages, as the support is withdrawn from the sol, further deposition occurs by dip-coating

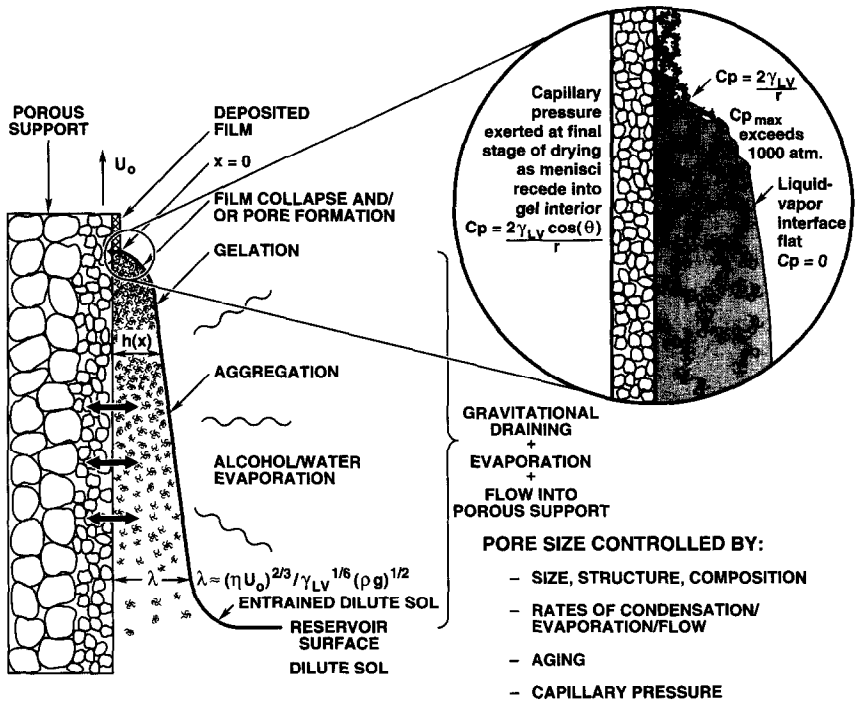

Fig. 1. Physical and chemical processes which contribute to film formation and pore size determination during membrane formation by dip coating/slip-casting of polymeric sols onto porous supports.

whereby sol entrained on the support is concentrated by evaporation leading to gelation and finally collapse of the gel network by capillary forces accompanying drying.

One strategy for the preparation of ultramicroporous membranes from polymeric sols relies on the concept of mutual transparency or opacity of fractal clusters. Mandelbrot [10] has shown that if two structures of radius r_c and mass fractal dimensions D_1 and D_2 are placed independently in the same region of space, the mean number of intersections $M_{1,2}$ is expressed as

$$M_{1,2} \propto r_c^{D_1+D_2-d} \quad (5)$$

where d is the dimension of space. Thus, in three dimensions, if each structure has a fractal dimension less than 1.5, the probability of intersection decreases indefinitely as r_c increases. The structures are mutually transparent: during membrane formation they should freely interpenetrate one another as they are forced into close proximity first by the increasing concentration and then by capillary forces accompanying drying (see Fig. 1). Alternatively if the mass fractal dimensions exceed 1.5, the probability of intersection increases with r_c. These structures are mutually opaque. During film or membrane formation, they do not interpenetrate as they are concentrated, so for opaque fractals, we expect that both the percent porosity and mean pore size of the membrane will increase with r_c as r_c^{3-D}.

This concept of mutual transparency or opacity was originally developed with the assumption that each point of intersection resulted in instantaneous and irreversible "sticking", chemically equivalent to an infinite reaction (condensation) rate. In practice the probability of sticking at each point of intersection is much less than unity and is influenced by catalyst concentration, temperature, and reactivity of the terminal ligands. For example, for silicate polymers prepared from tetraethoxysilane by a sol–gel process, the condensation rate is strongly dependent on the sol pH as estimated by the reciprocal gel times (see Fig. 2) [12]. If the probability of sticking at each point of intersection is reduced, transparency is increased, leading to denser films with smaller pore sizes.

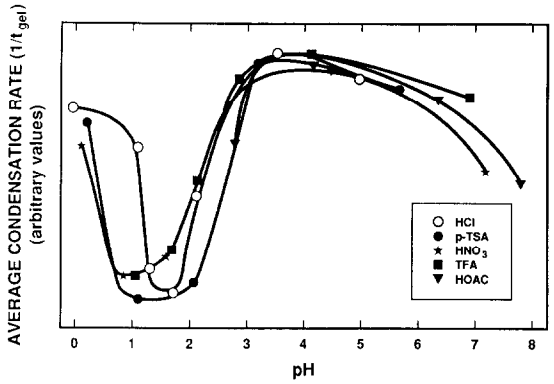

Fig. 2. Dependence of average condensation rates on pH for TEOS hydrolyzed with solutions of various acids: (*p*-TSA) *p*-toluenesulfonic acid; (HOAc) acetic acid; (TFA) tri-fluoroacetic acid. After Coltrain et al. [12].

This paper describes our strategy to prepare ultramicroporous supported membranes by deposition of mutually transparent silicate polymers under conditions where the condensation rate is minimized. In this situation the polymers should readily interpenetrate during deposition, and the network should remain compliant, promoting further reduction of the pore size by capillary forces exerted at the final stage of the drying process (see Fig. 1).

2. Experimental

2.1. Sol preparation and characterization

Silicate sols were prepared from tetraethoxysilane (TEOS) dissolved in ethanol using a two-step acid-catalyzed hydrolysis procedure (referred to as A2) [13]. In the first step TEOS, EtOH, H_2O, and HCl were combined in the molar ratios: $1.0:3.8:1.1:7.0\times10^{-4}$ and refluxed

at 60°C for 90 min. In the second step additional acid and water were added at room temperature resulting in the final molar ratios (TEOS:EtOH:H_2O:HCl): 1.0:3.8:5.1:0.06. To evaluate the effect of catalyst concentration a second sol was prepared with a final molar ratio of 1.0:3.8:5.1:0.026 (referred to as A2*). The sols were allowed to age at 50°C for periods ranging from 2 to 35 hr and then diluted 2:1 or 6:1 with ethanol (volume EtOH:volume sol). A schematic of the experimental matrix is shown in Fig. 3.

The effect of aging on silicate polymer structure was determined by small angle X-ray scattering (SAXS). SAXS data were collected using a Rigaku-SAXS setup having a Kratky U-slit system. The incident beam is Cu-Kα radiation with wavelength 0.1542 nm. Scattered X-ray intensity was counted with an MBraun position sensitive detector system. The data were then corrected for slit collimation in order to evaluate the radius of gyration and the fractal dimension by analysis of the Guinier and Porod regions of scattering, respectively.

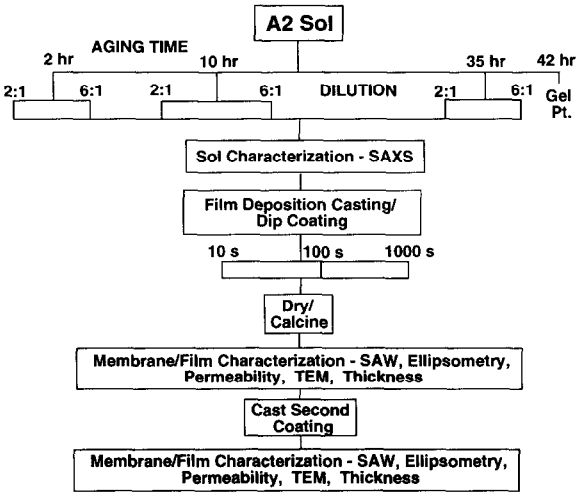

Fig. 3. Experimental matrix for preparation and characterization of sols and membranes.

2.2. Sol deposition

After aging and dilution the sols were cast on asymmetric tubular alumina supports supplied by Alcoa (now supplied by U.S. Filter). The supports were composed of four layers of successively smaller particles (three α-Al_2O_3 layers and one γ-Al_2O_3 inner layer), causing the pore size to vary from about 10 μm at the outside diameter to 4.0 nm at the inside diameter. The wall thickness was ~2 mm and the OD was ~10 mm. The tubular supports were cut into 5 cm segments with a diamond wafering saw, cleaned with CO_2 "snow", and outgassed in He at 150°C prior to membrane deposition. The outgassed tubes were mounted on a linear translation stage in a dry box and lowered into the sol at a rate of 20 cm/min. After immersion periods of 10, 100 or 1000 sec, the supports were withdrawn at a rate of 20 cm/min and allowed to dry in a flowing N_2 ambient for a period of 15 min. Companion samples were prepared by dip-coating the polymeric sols on solid ⟨100⟩ single crystal silicon wafers or single crystal quartz SAW substrates. The deposited membranes and films were calcined in air at a rate of 1°C/min to 400°C, maintained at 400°C for 10 min, and cooled to room temperature.

2.3. Structural characterization

X-ray fluorescence

Broken fragments of the coated supports were examined by a micro X-ray fluorescence method (Fisions/Kevex Omicron EDS Analyzer) to determine the areal averaged silicon content of the composite membrane/support structure. Micro-spot analysis was used to avoid errors due to curvature effects. Silicon content per unit area was converted to thickness by assuming that all the silicon was contained in a discrete silicate layer of density 2.0 g/cm^3.

Transmission electron microscopy (TEM)

TEM of the samples was performed to determine thickness, uniformity, defects, and morphology of the membrane layer. Broken fragments of the membrane/support structure used for X-ray fluorescence analysis were then mounted on fused silica cylinders such that the membrane layer was adjacent to the fused silica surface. These samples were sectioned with a diamond wafering saw, ground and polished to a thickness of about 1 μm, and ion milled to a thickness of several hundred angstroms. TEM was performed using a Philips Model CM-30 300 KV analytical instrument equipped with a LINK EDS analyzer.

Ellipsometry

Thickness and refractive index of companion thin film samples deposited on Si wafers were measured using a Rudolph Model AUTOELIV ellipsometer by assuming an absorption coefficient of 0.

Surface acoustic wave (SAW) sorption studies

A surface acoustic wave (SAW) technique was used to obtain N_2 and CO_2 absorption–desorption isotherms of ~ 1 cm^2 areas of films deposited directly on piezoelectric SAW substrates by either dipping or spinning. The piezoelectric ST-cut quartz oscillator, with an automatic gain control loop, in conjunction with a custom sample holder were incorporated into a Micromeritics ASAP 2000 gas adsorption analyzer. The frequency was measured by an Optoelectronics Model PC10/AP10H Universal Frequency Counter.

2.4. Transport measurements

Single-gas permeabilities of the uncoated support and coated membranes were measured as a function of pressure using He, N_2, O_2, and CO_2. The tubular membrane was supported in a gas flow cell, so that compression of viton gasket material at the ends of the membranes prevented bypassing. Compressed pressure-regulated gas at room temperature was flowed into the annulus of the membrane, with the flow rate set using a mass flow controller, and exited at the outside of the membrane. The pressure drop across the membrane was measured using pressure gauges, and the average pressure across the membrane could be varied using a valve downstream from the flow cell. The methodology employed for the permeability measurements was as follows. Membranes or uncoated supports were loaded into the flow cell and outgassed at approximately 150°C for 8 hr with a continual He flow of ~ 10 cm^3/min. The flow cell and membrane were then allowed to cool to room temperature before beginning the permeability measurements. The permeability measurements were then conducted by measuring the pressure on both sides of the membrane as a function of the steady-state mass flow rate permeating the membrane.

3. Results and discussion

3.1. Sol aging studies

Porod plots of the SAXS data are shown in Fig. 4 for the A2 sol after different periods of aging (2–35 hr) corresponding to normalized t/t_{gel} values of 0.05–0.92. Also shown is the scattering curve of the A2* sol prepared with a lower acid concentration and aged for 2 hr corresponding to $t/t_{gel}=0.03$. Aging causes both the polymer size and mass fractal dimension to increase as denoted by increasing values of the Guinier radii ($R_G=1.3$–2.6 nm) and decreasing values of the Porod slope $P(P=-D)$ measured at the high q limit, respectively. (See also Table 1). The reduction in acid concentration was observed to increase the gel time consistent with a reduction in the average condensa-

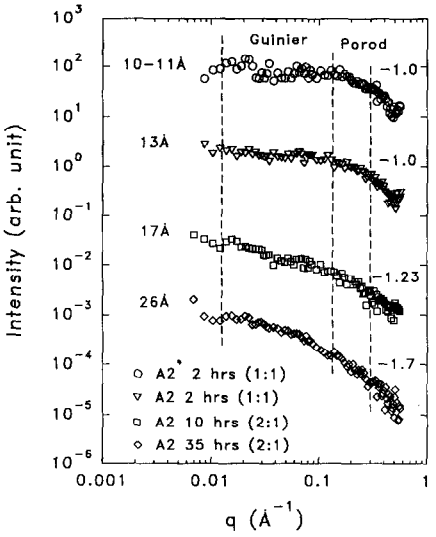

Fig. 4. Small angle X-ray scattering (SAXS) results for A2 and A2* silica sols after different aging times. Values presented on the scattering curves indicate the radius of gyration and the Porod slope. Dotted lines indicate the range over which R_G and Porod slope were calculated.

tion rate. Correspondingly R_G is observed to be slightly less for the A2* sol after 2 hr of aging than observed for the standard A2 sol.

Based on eqn. (5) and the associated discussion of mutually transparent fractals, we expect that, although D increases above 1.5 with 35 hr of aging, the polymers should be mutually transparent for all aging conditions, because the condensation rate is minimized within the pH range studied (pH 1–2, see Fig. 2).

3.2. *Thin film characterization*

Cross-sectional TEM at magnifications of 450×10^3 and 1×10^6 showed the A2 silicate membranes deposited on γ-Al_2O_3 supports to be featureless and crack free for all aging times and deposition conditions. See, for example, Fig. 5(a). Although the measured R_G for some sols was less than the pore radius of the support, EDS analysis identified only minor amounts of Si within the support to a depth of about 10–100 nm, depending on conditions. Most likely, continued condensation reactions and/or increasing viscosity resulting from sol concentration during membrane deposition inhibits penetration. Film thicknesses for these membranes measured from the TEM micrographs ranged from about 10 to 120 nm depending on conditions (see Table 1) and were observed to vary significantly from one region of a sample to another. This may be a result of nonuniformities in the thickness and/or pore structure of the underlying γ-Al_2O_3 support which affect the casting rates.

TEM micrographs of the membrane prepared from the A2* sol catalyzed with 0.44 N acid revealed no distinct membrane layer (see Fig. 5b), and EDS indicated penetration of the Si to a depth of over 1 μm into the support layer. Presumably due to a reduced condensation rate, this sol was apparently able to penetrate relatively freely into the support during membrane casting even though the R_G for the A2* sol was only slightly less than that of the comparable A2 sol after 2 hr of aging. Transport measurements, discussed in detail below, indicated a much lower permeation rate for the membrane prepared from the A2* sol, probably due to either pore plugging of the 40 Å support layer, creating a membrane layer of greater effective thickness ($\leqslant 1$ μm), or possibly reduced pore size. These results are a further indication that condensation reactions that accompany membrane deposition play an important role in determining the nature and characteristics of the deposited membrane layer.

Thickness of the supported A2 silicate membranes determined by micro X-ray fluorescence (assuming all Si to be in a discrete layer of density 2.0 g/cm^3) ranged from 27–128 nm and generally increased with aging and casting times and decreased with dilution (Table 1).

The refractive indices of companion samples prepared by dip-coating ranged from 1.430 to 1.435 with no obvious dependence on aging

TABLE 1

Summary of characteristics of sols and deposited films and membranes

Sol conditions and characteristics				Deposition time (sec)	Film characteristics		
Aging time (hr)	Solvent dilution ratio	SAXS			Porous support	Ellipsometry (dense support)	
		R_g (Å)	D		XRF thickness (Å)	Refr. index	Thickness (Å)
A2							
2	1:1	13	1.0				
	2:1			100			
10	2:1	17	1.23	100		1.435	1247
	6:1			100	274		
				1000	392	1.432	537
35	2:1	26	1.7	100	1236	1.430	1423
	6:1			1000	816	1.431	583
A2*							
2	1:1	11	1.0				
	2:1			100			

times or dilution factors (Table 1). If we assume the siloxane skeleton to have a refractive index identical to fused silica (~ 1.45), these refractive indices are consistent with porosities of $<5\%$ according to the Lorentz–Lorenz analysis. Most likely the refractive index of the hydroxyl terminated siloxane skeleton exceeds 1.45, so the actual porosities are slightly greater than 5%. Though the properties of a membrane layer deposited on a porous support cannot generally be assumed to be the same as films deposited on dense substrates [8], due in part to different time scales of the deposition processes, the fact that the sols were prepared under conditions where the condensation rate is nearly minimized should greatly reduce differences between the membranes and companion films [14], allowing a reasonable estimate of the membrane properties.

Both the high refractive index values (low porosities) and the independence of refractive index on aging time are consistent with the concept of mutually transparent fractal polymers. During membrane deposition they interpenetrate to form a densely packed layer that is further compacted by the capillary pressure P_c exerted on the polymer network at the final stage of drying (see Fig. 1):

$$P_c = -2\gamma_{LV}\cos(\theta)/r_p \quad (9)$$

where γ_{LV} is the liquid–vapour surface tension, θ is the contact angle, and r_p is the pore radius. Interpenetration of the polymers leads to networks with very small pores causing P_c to be enormous, quite conceivably exceeding 1000 bars [14].

Figure 6 shows N_2 and CO_2 adsorption–desorption isotherms of a film prepared from an unaged A2 sol by spin-coating on a SAW substrate. The N_2 isotherm acquired at 77K is of Type II implying that there is no porosity accessible to N_2 molecules (kinetic diameter = 0.396 nm). The CO_2 isotherm acquired at $-78°C$ is of Type I suggestive of microporosity. Hysteresis is observed however (desorp-

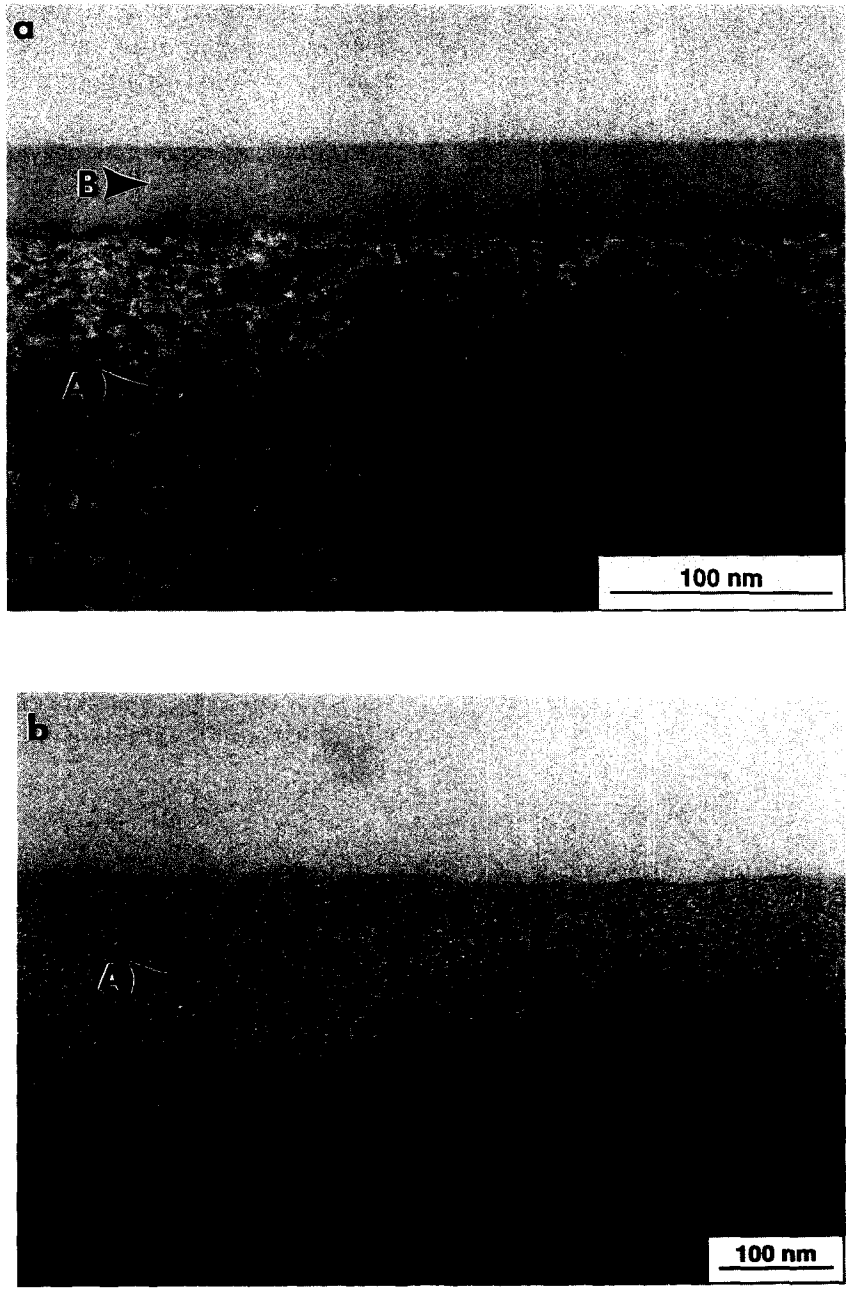

Fig. 5. (a) Cross-sectional TEM image of ultramicroporous SiO_2 membrane layer deposited on γ-Al_2O_3 membrane support. Region A indicates γ-Al_2O_3 support (40 Å) layer, B indicates the deposited SiO_2 layer. (b) Cross-sectional TEM image of SiO_2 membrane layer deposited from the A2* sol. In contrast to (a), this micrograph only shows one region, labeled A, which contains both Si and Al to a depth of > 1 μm by EDS analysis.

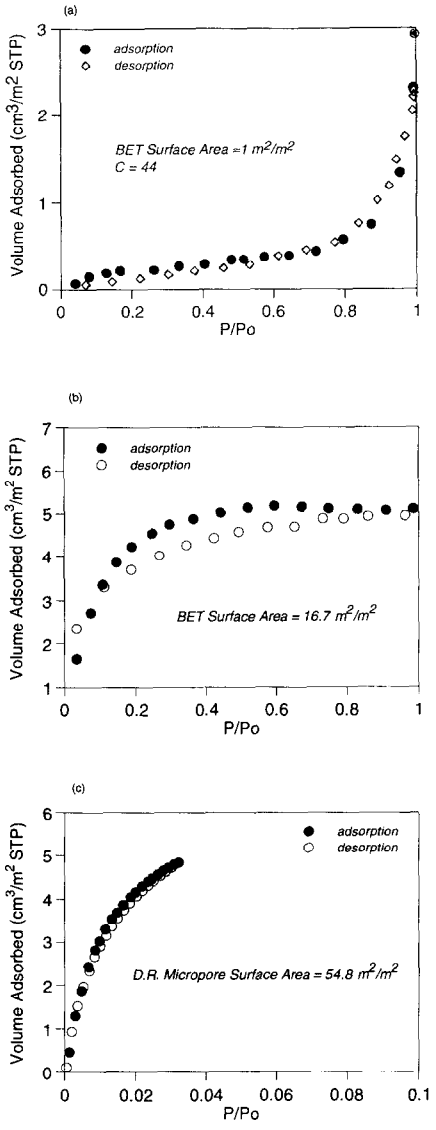

Fig. 6. N_2 and CO_2 adsorption-desorption isotherms of an unaged A2 sol film determined using the surface acoustic wave (SAW) technique on a film deposited by spin-coating on a SAW substrate. (a) N_2 at 77K, (b) CO_2 at 195 K, and (c) CO_2 at 273 K.

tion branch below adsorption branch), which we believe to be a result of non-equilibrium conditions. The limited CO_2 adsorption–desorption isotherm acquired at 0°C shows no hysteresis. Since the kinetic diameter of CO_2 (0.34 nm) is not too different from that of N_2, the different isotherm shapes presumably reflect kinetic limitations of adsorption at low temperatures in the small pores of the films.

3.3. Transport characterization

The permeability and ideal selectivity characteristics of membranes prepared using sols with different aging times, dilution ratios, and acid catalyst concentrations were investigated using single-gas (He, N_2, O_2, CO_2) permeation measurements. Much of the permeation data are reported in units of cm^3/cm^2-sec-cmHg (which we call "permeance"), rather than barrer units (1 barrer$=10^{-10}$ cm^3-cm/cm^2-sec-cmHg), because the appropriate layer thickness to apply is unclear in such a composite structure. Permeance, then, relates the measured permeation flux to the overall pressure driving force, and corresponds to the inverse of the total transport resistance. Thus, the measured flux can be expressed as

$$J\left(\frac{\text{cm}^3}{\text{cm}^2\text{-sec}}\right)=F_T\Delta P, \tag{7}$$

where F_T is the permeance of support plus coating(s).

Figure 7 shows the effect on He permeance

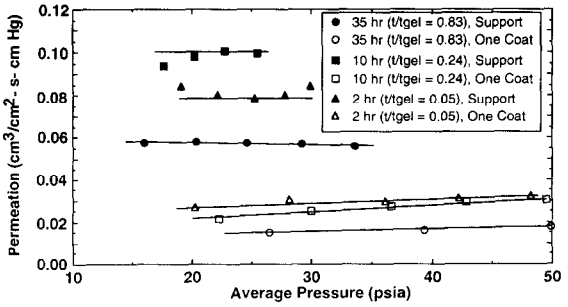

Fig. 7. Helium permeation measurements as a function of average pressure across the membrane for membranes prepared by depositing a single coating from A2 sols with different aging times (2:1 EtOH dilution, 100 sec dipping time, 1.0 N acid catalyst concentration).

of a single deposition from A2 sols with varied aging times, where the dilution ratio was kept constant (2:1) and casting time was 100 sec. There was considerable variability in the permeance of the support before coating, indicating variable thickness of the 40 Å support layer. Such variability was also implied by the non-uniform deposited layer thicknesses revealed by TEM. The percent reduction in permeance after coating with the 10 hr or 35 hr sols was essentially the same (75%), while the reduction for the 2 hr sol was slightly less (65%). This could be due to differences in pore size and/or the deposited layer thickness for the different sols. A second membrane coating was also deposited from the A2 sols after 10 and 35 hr of aging. The He permeation results following the second coating were considerably different in nature. The second coating led to relatively little further reduction (~15%) in permeance for the 10 hr sol, while the percent reduction for the second coating of the 35 hr sol was comparable to that observed with the first coating (~75%). The coating behavior with multiple depositions is still under investigation.

Before coating permeance was essentially independent of pressure, which is consistent with Knudsen transport, whereas after coating a slight pressure dependence was sometimes observed. The slight pressure dependence after coating could be due to an increased surface diffusion component, or could be due to a small amount of viscous transport (e.g. due to leakage at the tube ends) which becomes relatively more apparent with the reduced permeability after coating. Higher temperature transport measurements are planned to measure activated transport which, together with further transport calculations, should resolve this issue.

Nitrogen permeances were also measured for the membranes in Fig. 7, and the percent permeance reductions were very similar to those found for He. These results are given in Table 2 in terms of the ideal He/N_2 selectivities. The changes in selectivity with membrane coating must be considered insignificant, except perhaps for the case of the 2 hr-aged A2 sol. The fact that substantial reductions in permeability occurred with membrane deposition, but with essentially no change in the He/N_2 selectivity, indicates that the deposited layers had considerably reduced pore sizes; but the pore sizes were apparently not reduced to the level of He/N_2 molecular size exclusion. Further implications of the pore size reductions implied by such decreases in permeation rate are discussed further below. Though the magnitude of He/N_2 selectivities observed is consistent with non-

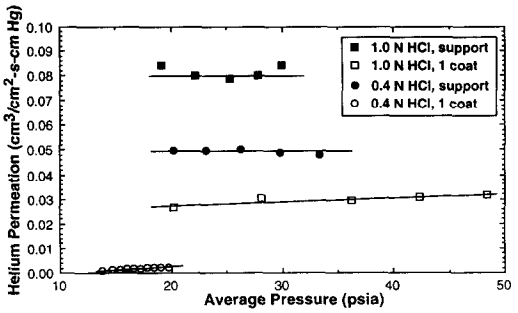

Fig. 8. Helium permeation measurements as a function of average pressure across the membrane for membranes prepared by depositing a single coating from A2 (1.0 *N* acid concentration) and A2* (0.44 *N* acid concentration) sols aged for 2 hr.

TABLE 2

Summary of ideal He/N_2 selectivities measured on membranes prepared from different sols. (Ideal Knudsen $\alpha_{He/N_2} = 2.65$)

Sol	Aging time (hr)	Ideal He/N_2 selectivity (α_{He/N_2})		
		Support	1 coat	2 coats
A2 (2:1, 100 sec)	2	2.0	1.5	
	10	1.7	1.5	1.6
	35	2.2	2.0	2.0
A2* (2:1, 100 sec)	2	1.7	1.5	

ideal Knudsen separation, they may also be due to other molecular-size-dependent separation mechanisms. O_2 and CO_2 permeances were also measured for supports and some coated tubes, and selectivity factors involving them (e.g. N_2/O_2, N_2/CO_2, etc.) were also typically slightly below the ideal Knudsen values, and changed only slightly with membrane deposition.

The acid catalyst concentration employed during sol preparation was found to have a dramatic effect on the permeation of deposited membrane layers. The effects of a single membrane coating using A2 and A2* sols catalyzed with 1.0 *N* and 0.44 *N* HCl, respectively, are compared in Fig. 8. The lower catalyst concentration (0.44 *N*) led reproducibly to considerably larger reductions in permeance than were observed using a 1.0 *N* concentration (a ~95% reduction in He and N_2 permeance compared to ~60%). This result is still being investigated, but is probably a consequence of the strong pH sensitivity of the condensation rate near its minimum around pH=2 (Fig. 2). The slightly smaller R_G measured by SAXS (Table 1) for the 0.44 *N* sol is consistent with a lower condensation rate during sol preparation. A lower condensation rate during deposition should reduce the tendency for gel formation at the support interface and promote penetration of small polymers ($R_G \leqslant 10$ Å) into the 40 Å support (see Fig. 5b) resulting in substantially thicker films ($\leqslant 1\ \mu m$) for equivalent amounts of silicate deposition.

3.4. Analysis of permeability measurements

If the permeation rates are independent of average pressure, then the permeance of the deposited membrane layer material alone can be easily decoupled from the measured overall permeance using the relationship

$$\frac{1}{F_T} = \frac{1}{F_S} + \frac{1}{F_m}, \tag{8}$$

where F_m is the permeation of the deposited layer, F_S is the support permeance and F_T is the measured overall permeance. Thus, from the data in Figs. 7 and 8, the permeance of the deposited layer can be determined (neglecting the slight pressure dependence sometimes seen in the coated membranes). The intrinsic permeability of the deposited material can then be estimated by multiplying the permeance by the approximate deposited layer thickness. The permeabilities thus calculated (where permeances were determined at 20 psia) for the membranes in Figs. 7 and 8 are summarized in Table 3. No estimates were made for the 2 hr-aged sols or the double-coated membranes because the layer thicknesses were not known for them. The permeabilities for the 35 hr and 10 hr-aged sol membrane coatings were roughly equal and approximately 100 times lower than the permeability of the 40 Å layer of the support. Though the layer thicknesses of the 2 hr-aged sol coatings were not determined by TEM or XRF, if the same intrinsic permeability as the 10 hr 2:1 A2 sol is assumed for the 2 hr A2 coating, a layer thickness of 400 Å is calculated. This thickness is physically consistent with accumulation of smaller polymers on the outside of the support. If the same calculation is performed for the 2 hr-aged A2* sol deposit, the calculated layer thickness is 0.6 μm. Such a large predicted layer thickness is consistent with penetration of the sol into and partially filling the pores of the support 40 Å layer. This is consistent with cross-sectional TEM of the A2* membrane which showed no external silicate layer, but which revealed (by EDS) Si penetration down to ~1 μm into the support.

The magnitude of the permeance reduction which occurred with membrane coating can also be used to provide a rough idea of the pore size range of the deposited material. Since the transport resistance of the support is dominated by the 40 Å Knudsen transport layer, the flux through the uncoated support can be rep-

TABLE 3

Summary of permeance and permeability of helium for deposited membrane layers (permeance data taken at 20 psia)

Sol (aging time, dil. ratio, coating time)	Permeance (cm^3/cm^2-sec-cmHg)			Membrane layer thickness (Å)	Permeability (barrer)[a]
	Support (F_S)	Single-coated support (F_T)	Deposited membrane layer (F_M)		
35 hr, 2:1, 100 sec	0.05755	0.015	0.0203	1200 (XRF)	2400
10 hr, 2:1, 100 sec	0.10	0.022	0.0282	600 (est.)	1600
2 hr, 2:1, 100 sec (1.0 *N* acid)	0.0795	0.027	0.0409	?	?
2 hr, 2:1, 100 sec (0.44 *N* acid)	0.0495	0.0025	0.0026	?	?

[a] 1 barrer = 10^{-10} cm^3-cm/(cm^2-sec-cmHg).

resented approximately by the Knudsen transport flux relationship

$$J_K\left(\frac{cm^3}{cm^2\text{-sec}}\right)= \frac{P_{std}}{RT_{std}}\frac{4\epsilon r_p}{3\tau_K}\left[\frac{2}{RT\pi M}\right]^{1/2}\frac{\Delta P}{\Delta a}=F_S\Delta P \qquad (9)$$

where r_p is the pore radius, ϵ is the porosity, τ_K is the tortuosity, M is molecular weight, Δa is the layer thickness, F_S is the permeance, and P_{std} and T_{std} are the standard gas pressure and temperature. With the deposition of an additional layer the same flux would flow through each layer. If the additional layer could also be characterized by Knudsen transport, then setting the flux expressions for each layer (eqn. 9) equal and rearranging yields an expression which relates the pore radii of the two layers to the permeance measured before (F_1) and after (F_{1+2}) the additional layer was deposited:

$$\frac{r_{p2}}{r_{p1}}=\frac{\epsilon_1\tau_2}{\epsilon_2\tau_1}\frac{\Delta a_2}{\Delta a_1}\frac{F_{1+2}}{F_1-F_{1+2}}. \qquad (10)$$

For the Alcoa 40 Å layer, resonable values for the parameters are $\epsilon_1=0.50$, $\tau_1=3$, $\Delta a_1=5$ μm, and $r_{p1}=20$ Å [15,16]. Values for the polymeric silica layer are less certain, but they probably lie in the following ranges based on data presented herein and our experience with films on dense substrates: $\epsilon_2=0.05$–0.15, $\tau_2=3$–5, $\Delta a_2\approx 500$–1000 Å. Using these values and taking the permeance reduction upon membrane deposition to be 50% [$F_{1+2}/(F_1-F_{1+2})=1$], the radius of the deposited layer is predicted to be $r_{p2}/r_{p1}=0.033$–0.33. This would correspond to a pore radius on the deposited layer of 0.7–7.0 Å. This range is consistent with the analysis of SAW device adsorption measurements. Larger permeance reductions would indicate even smaller r_{p2}. This analysis demonstrates that the magnitude of permeability reductions observed after membrane deposition from the polymeric sols can only be explained by pore radii smaller than 10 Å, where the application of Knudsen transport theory becomes questionable. The fact that the ideal selectivities measured thus far are essentially Knudsen-like in magnitude indicates that transport in the deposited layer is molecular size dependent (molecular sizes roughly correlate with molecular weights), but pore sizes are not small

enough to observe a molecular sieving effect with the molecules used. Experiments are planned to utilize larger gas probe molecules to test this idea.

4. Summary and conclusions

Commercial alumina membranes with a 40 Å pore diameter separation layer were used as supports for the deposition of thin (200–1000 Å), defect-free ultramicroporous (pore radius <10 Å) silica layers from acid-catalyzed silicate sols. Acid catalyst concentration, which governs the polymer condensation rate, and aging time of the sols were changed to provide sols which were unable to penetrate the support 40 Å layer and accumulated in a defect-free layer on the surface, or which penetrated into the 40 Å support leading to partial pore plugging. The condensation rate, determined by catalyst concentration, plays an important role in both polymer penetration and membrane formation, since condensation reactions continue to occur during membrane deposition and drying. Under conditions of minimal polymer penetration, sol aging time, solvent dilution, and casting/dipping time affect the thickness of the deposited membrane layer.

The deposited silica membrane layers had He permeabilities of 1000–2000 barrer, causing a reduction in the overall permeability of the composite membrane by 65–90% depending on conditions. Calculations based on measured reductions in permeation rate and measured layer thicknesses indicated a pore radius of less than 10 Å for the deposited membranes. This was consistent with SAW adsorption (N_2, CO_2) characterization of the films on dense supports. Permeability measurements using He, N_2, O_2 and CO_2 at room temperature gave ideal selectivities slightly below Knudsen values. Thus, the deposited membrane layers were concluded to be ultramicroporous, but with a pore size too large to provide molecular sieving with these probe molecules. Further experiments are planned to elucidate the transport mechanisms in the ultramicroporous membranes, as well as to manipulate the condensation rate and aging time to produce membrane layers with smaller pore sizes and molecular sieving properties.

Acknowledgments

Portions of the work were supported by the Electric Power Research Institute, the National Science Foundation, the Gas Research Institute, and the Department of Energy – Morgantown Energy Technology Center. In addition, we are grateful to T. Tribble of Sandia National Laboratories for the TEM sample preparation and analysis, and R.G. Tissot of Sandia National Laboratories for the X-ray micro fluorescence analysis. Sandia National Laboratories is a U.S. Department of Energy facility supported by DOE Contract Number DE-AC04-76-DP00789.

References

1 R.R. Bhave, Inorganic Membranes Synthesis, Characteristics and Applications, Van Nostrand Reinhold, New York, NY, 1991.
2 A.F.M. Leenaars, K. Keizer and A.J. Burggraaf, The Preparation and characterization of alumina membranes with ultra-fine pores. Part 1. Microstructural investigations on non-supported membranes, J. Mat. Sci., 10 (1984) 1077-1088.
3 A. Larbot, J.A. Alary, J.P. Fabre, C. Guizard and L. Cot, Microporous layers from sol-gel techniques, in: C.J. Brinker, D.E. Clark and D.R. Ulrich (Eds.), Better Ceramics through Chemistry II, Mat. Res. Soc., Pittsburgh, PA, 1986, p. 659.
4 M.A. Anderson, M.J. Geiselmann and Q. Xu, Titania and alumina ceramic membranes, J. Membrane Sci., 39 (1988) 243-258.
5 G.D. Parfitt, Fundamental aspects of dispersion, in: Dispersion of Powders in Liquids, 3rd edn., Applied Science, London, 1981, pp. 1-50.
6 T.J. Garino, Patterning, drying and sintering of particle films on rigid substrates, Ph.D. Dissertation, M.I.T., Cambridge, MA, 1986.
7 B.E. Yoldas, A transparent porous alumina, Am. Ceram. Soc. Bull., 54 (1975) 286-288.

8 C.J. Brinker and G.W. Scherer, Sol-Gel Science, Academic Press, San Diego, CA, 1990.
9 P. Meakin, Formation of fractal clusters and networks by irreversible "diffusion-limited" aggregation, Phys. Rev. Lett., 51 (1983) 119.
10 B.B. Mandelbrot, The Fractal Geometry of Nature, Freeman, San Francisco, CA, 1982.
11 C.J. Brinker, G.C. Frye, A.J. Hurd and C.S. Ashley, Fundamentals of sol-gel dip coating, Thin Solid Films, 201 (1991) 97-102.
12 B.K. Coltrain, S.M. Melpolder and J.M. Salva, in: D.R. Uhlman and D.R. Ulrich (Eds.), Ultraprocessing of Ceramics, Glasses and Composites, Wiley and Sons, New York, NY, 1992, pp. 69-76.
13 C.J. Brinker and G.W. Scherer, Sol-Gel Science, Academic Press, San Diego, CA, 1990, p. 110.
14 C.J. Brinker, A.J. Hurd, G.C. Frye, P.R. Schunk and C.S. Ashley, Sol-gel thin film formation, J. Ceram. Soc. Jpn., 99 (1991) 862-876.
15 H.P. Hsieh, R.R. Bhave and H.L. Fleming, Microporous alumina membranes, J. Membrane Sci., 39 (1988) 221-241.
16 K. Keizer, R.J.R. Uhlhorn, R.J. Van Vuren and A.J. Burggraaf, Gas separation mechanisms in microporous modified γ-Al_2O_3 membranes, J. Membrane Sci., 39 (1988) 285-300.